Author/s:
Strecker, T;Aarsnes, UJF

Title:
Boundary Control and Estimation for Underbalanced Drilling With Uncertain Reservoir Parameters

Date:
2023-01-01

Citation:
Strecker, T. & Aarsnes, U. J. F. (2023). Boundary Control and Estimation for Underbalanced Drilling With Uncertain Reservoir Parameters. IEEE TRANSACTIONS ON CONTROL SYSTEMS TECHNOLOGY, 31 (1), pp.281-294. https://doi.org/10.1109/TCST.2022.3178039.

Persistent Link:
https://hdl.handle.net/11343/333312

Boundary Control and Estimation for Under-Balanced Drilling with Uncertain Reservoir Parameters

Timm Strecker, Ulf Jakob F. Aarsnes

***Abstract*— In under-balanced drilling, the bottom-hole pressure is kept below pore pressure, causing pressure dependent influx of reservoir gas into the wellbore that makes the system unstable at low drawdowns. In this paper we propose a feedback controller which stabilizes the system, represented by the "reduced Drift Flux Model", around an arbitrary pressure setpoint, while using only topside measurement and assuming unknown reservoir parameters. A particular challenge with this problem is the distributed and highly nonlinear nature of the system dynamics, where the "reduced Drift Flux Model" models gas-liquid flow as a nonlinear transport equation with a non-local integral source term. An observer estimates the distributed gas concentration, downhole pressure, and reservoir parameters by solving the system dynamics backwards relative to how the gas rises in the well. The control inputs are then constructed by designing target states over the next sampling period and again solving reversed dynamics to obtain the required topside pressures. The resulting controller is implemented with a 2 minute zero-order hold to accommodate the actuation limitation situation on an actual drilling rig. Finally, the results are illustrated in simulations with an industry standard Drift Flux formulation as the plant model.**

***Index Terms*— Under-balanced drilling, partial differential equations, boundary control, observer, parameter estimation, distributed parameter systems, adaptive control**

I. Introduction

When drilling a well for the purpose of producing hydrocarbons, a slim borehole is created into a permeable pressurized formation using a drilling bit attached to a drill string. Drilling liquid is injecting into the top of the drill string and flows out through the drill bit and up the annulus around the drill string carrying formation cuttings with it out of the borehole, see Fig. 1. Controlling the pressure of the drilling fluid near the bottom of the well is of key importance to the success of the drilling operation: Too high pressure means that expensive drilling liquid is lost to the formation which results in reduced return flow and insufficient hole cleaning. Too low pressure can result in pressurized formation fluids entering the well, displacing the high density drilling liquid, and creating an unstable feedback loop which can result in blow-out and collapse of the well if not controlled [1], [2].

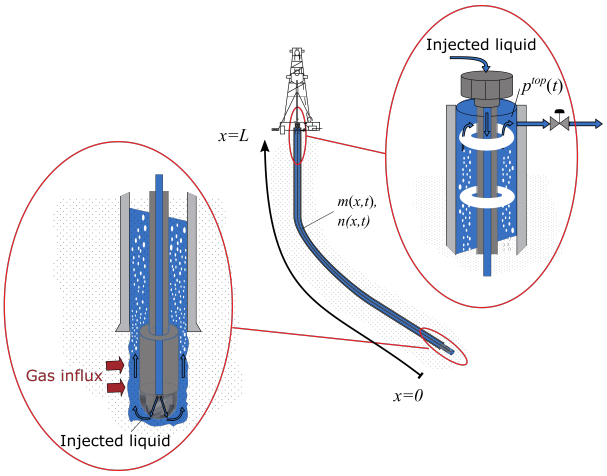

Fig. 1. Schematic of an underbalanced well being drilled.

To control the pressure in the well more effectively, many wells are today drilled with a sealed anulus and a manipulated back-pressure choke, which allows for the control of the pressure at the top of the well by the driller. In particular, these tools are used to perform *Under-Balanced Drilling* (UBD) where the well pressure is intentionally kept below the formation pore pressure such that formation fluids flow into the well while drilling. Underbalanced drilling have many benefits, such as improved rate of penetration, better cuttings transport, higher well productivity and less risk of loss of drilling liquid [3]. However, these benefits come at the cost of the significant increase in the difficulty of controlling the well [4].

In the context of automated pressure and flow control, the dynamics of the two-phase flow encountered in UBD is significantly more complicated than the single-phase flow of conventional drilling: In single-phase flow any operating point is inherently stable, transients are short and predictable and, barring certain well control incidents, operating conditions are reasonably homogeneous. By contrast, in two-phase underbalanced operations, the distributed gas–liquid flow and the reservoir–well interaction result in classical nonlinear behavior such as multiple equilibria, limit cycles and bifurcations as described by [5]–[7].

A particular challenge with UBD is the interaction between

This work was supported by the Australian Research Council (LP160100666) and the Research Council of Norway through the research center DigiWells (309589) at NORCE.

T. Strecker is with the Department of Electrical and Electronic Engineering, The University of Melbourne, Australia (timm.strecker@unimelb.edu.au).

U. J. F. Aarsnes is with NORCE Norwegian Research Centre AS, Oslo, Norway (ulaa@norceresearch.no) .

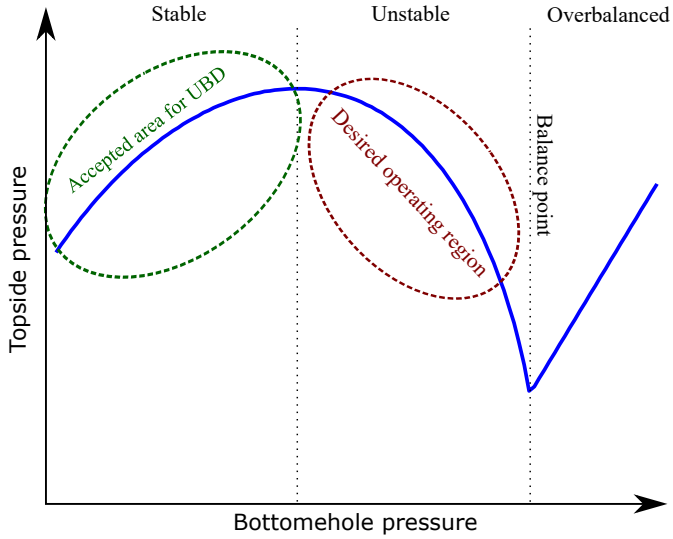

Fig. 2. Conceptual plot showing the relation between topside and bottomhole pressures at equilibrium. For a given topside pressure there are typically three equilibrium points: one overbalanced, one open loop *unstable* underbalanced, and one open loop stable underbalanced.

the well and the reservoir, wherein a low well pressure induces reservoir influx of low density fluids which displaces the high density drilling liquid reducing the hydrostatic pressure causing yet more influx. This positive feedback loop makes the well unstable at a wide range of bottomhole pressures below the balance point, see Fig. 2. To have stable operation in open loop, sufficient influx is required such that the frictional pressure loss caused by the influx becomes greater than the reduction in the hydrostatic pressure. Consequently, UBD is currently limited to formations with very high collapse pressure-margins. As such, there is a significant value proposal in using automated pressure control to stabilize the open loop unstable region below the balance point [8], [9].

However, the non-linear and distributed nature of the system makes controller design challenging. The necessity to control the system from a stable to an open loop unstable equilibrium with vastly different dynamics (from one-phase overbalanced to two-phase underbalanced flow) precludes the application of standard "off-the shelf" linearized controller-designs. As such, this problem motivates the distributed non-linear controller design approach pursued in the present paper where we focus on the stabilization problem which has not been explicitly adressed before. We refer to the following papers on MPC and linear multivariable control of the extended drilling process for additional context: [10]–[13]. Approaches in the literature to the control of PDEs include backstepping [14]–[18] and PI [19]–[24] controllers. However, the non-linearity of the model and that only infrequent (if any) downhole measurements are available disqualifies these methods in this case.

The proposed sampled-time output feedback controller consists of an observer and a feedback controller. The observer estimates the current distributed gas concentration in the well based on the history of topside measurements only, i.e., without requiring any downhole measurements of pressure or other variables. The feedback controller maps the estimate of the current gas concentration and the reference for the bottom hole pressure, into the topside pressures that are required to achieve the desired reference. The proposed control law is model based, and takes into account the distributed non-linear dynamics, including non-local dependencies of the terms modelling gas expansion which depend on the weight of the whole fluid column. In simulations with a more detailed drift-flux model, the proposed control law stabilizes the system in the desired operating region below the pore pressure, see Fig 2. Specifically, we choose a operating point just below the balance point, which is considered the most difficult region to operate in. Moreover, the proposed estimation scheme allows the online identification of uncertain reservoir parameters determining the gas influx, again based solely on topside measurements. This allows the adaptation of the controller while the system is operated in closed-loop control.

The proposed observer is related to the approach in [25] where, starting with the history of topside measurements, the model dynamics are first solved backwards to reconstruct the past gas and pressure distribution in the well, which is then used to estimate the current state in a second step. The feedback control part builds on ideas presented in [26]–[29], where one starts with the reference signal and again solves the distributed, non-linear model dynamics backwards to determine the inputs that are required to achieve reference tracking. However, these references consider different classes of systems without the non-local dependencies. In that sense, the theoretical contributions of this paper can be seen as an extension of this approach to a class of quasilinear hyperbolic partial differential equations (PDEs) with non-local source terms.

II. Modelling

In this section we describe the Drift-Flux Model (DFM) that we will use to simulate the plant, and then the reduced-DFM that we use for the model based control design.

A. Drift-flux model

As the plant model, to represent the two-phase gas–liquid flow and pressure dynamics, we use the drift-flux model presented in [30] (see [31] for numerical details). The drift-flux model is an established way to represent two-phase flow in drilling in the litterature [32], [33]. Define the mass variables

$$m = \alpha_L \rho_L, \qquad n = \alpha_G \rho_G, \tag{1}$$

where for $k = L, G$ denoting liquid or gas, ρ_k is the density and α_k is the volume fraction of the respective phase. Let p be the pressure and v_k be the velocity of each phase. All variables above depend on time $t \geq 0$ and spatial position $x \in [0, L]$ along the well (in curvilinear coordinates, where $x = 0$ corresponds to the well bottom and $x = L$ is at the topside choke), but the arguments (x, t) behind the variables are often omitted for readability, see schematic in Fig. 1. The distributed mass balances for the two phases and the momentum balance

for the mixture are given by

$$\frac{\partial m}{\partial t} = -\frac{\partial (m v_L)}{\partial x}, \tag{2}$$

$$\frac{\partial n}{\partial t} = -\frac{\partial (n v_G)}{\partial x}, \tag{3}$$

$$\frac{\partial (m v_L + n v_G)}{\partial t} = -\frac{\partial (m v_L^2 + n v_G^2)}{\partial x} - \frac{\partial p}{\partial x} - F - G. \tag{4}$$

In (4), the gravity term is $G = (m+n) g \cos(\phi)$ where g is the gravitational acceleration and ϕ is the inclination from vertical. The friction term is $F = \frac{f \rho v_m |v_m|}{D}$, with friction factor f, mixture density $\rho = m + n$, mixture velocity $v_m = \alpha_L v_L + \alpha_G v_G$ and hydraulic diameter D.

The model is completed by the following algebraic relations. The volume fractions add up to one, i.e.,

$$\alpha_L + \alpha_G = 1. \tag{5}$$

The densities depend on the pressure as given in

$$\rho_L = \rho_{L,0} + \frac{p}{c_L^2}, \qquad \rho_G = \frac{p}{c_G^2}, \tag{6}$$

where $\rho_{L,0}$ denotes the liquid density in vacuum, and c_L, c_G the speed of sound in liquid and gas, respectively. The velocities satisfy the slip law

$$v_G = C_0 v_L + v_\infty, \tag{7}$$

where C_0, v_∞ are empirical slip parameters discussed in [34]. In this model, the pressure is well-defined and can be obtained by solving (1) with (5)-(6) for p. For simplicity and readability, we omitted any spatial dependence of the parameters (f, c_L, etc.), but all parameters can be made dependent on x (e.g., due to temperature variations along the well) without any change in the proposed approach.

B. Boundary conditions

In this paper we assume that the pressure applied at the topside choke is a manipulated variable determined by the driller or a control law, i.e.,

$$p(L,t) = p^{\text{top}}(t), \tag{8}$$

with p^{top} as the manipulated variable. At the well bottom, the gas inflow depends on the difference between bottomhole pressure and the reservoir pore pressure. In this paper, we use

$$An(0,t) v_G(0,t) = k_G \max(0, p_{\text{res}} - p(0,t)), \tag{9}$$

where A is the cross section of the annulus and k_G is the gas production index, although it is straightforward to generalize the methods presented in this paper to other nonlinear relationships. The amount of liquid injected through the bit at the well bottom, $W^{L,inj}$, is determined by the rig pump

$$Am(0,t) v_L(0,t) = W^{L,inj}(t). \tag{10}$$

C. Simplified model for control design

In order to make the model more amenable for model-based control design, a simplification of the drift-flux model has been proposed in [35]. Observing that the pressure dynamics in the well are magnitudes faster than the transport of mass, a quasi-equilibrium assumption is imposed on the momentum balance (4), so that the number of distributed equations can be reduced to just one for the continuity of the gas volume fraction.

Using this approach, the gas volume fraction can be approximated as

$$\frac{\partial \bar{\alpha}_G}{\partial t} + \bar{v}_G \frac{\partial \bar{\alpha}_G}{\partial x} = \bar{E}_G, \tag{11}$$

where the term

$$\bar{E}_G = -\frac{\bar{\alpha}_G (1 - C_0 \bar{\alpha}_G) \bar{v}_G}{\bar{p}} \frac{\partial \bar{p}}{\partial x} \tag{12}$$

accounts for gas expansion as the pressure decreases higher up in the well. In this simplified model, the gradient of the velocity $\bar{v}_G$ and the pressure $\bar{p}$ are

$$\frac{\partial \bar{p}}{\partial x} = -(\bar{G} + \bar{F}), \qquad \frac{\partial \bar{v}_G}{\partial x} = -\frac{C_0 \bar{\alpha}_G \bar{v}_G}{\bar{p}} \frac{\partial \bar{p}}{\partial x}, \tag{13}$$

where $\bar{F} = \frac{f \bar{\rho} \bar{v}_m |\bar{v}_m|}{D}$, $\bar{G} = \bar{\rho} g \cos(\phi)$, $\bar{\rho} = \bar{\alpha}_G \bar{\rho}_G + (1 - \bar{\alpha}_G) \bar{\rho}_L$, and $\bar{\rho}_G$ and $\bar{\rho}_L$ are as in (6) but with $\bar{p}$ instead of p. Using this, the pressure and velocity profiles can be obtained by starting from either the topside or the bottomhole pressure and velocity, respectively, via

$$\bar{p}(x,t) = \bar{p}(L,t) + \int_x^L \bar{G}(\xi,t) + \bar{F}(\xi,t) d\xi, \tag{14}$$

$$\bar{v}_G(x,t) = \bar{v}_G(L,t) - \int_x^L \frac{\partial \bar{v}_G(\xi,t)}{\partial \xi} d\xi, \tag{15}$$

or

$$\bar{p}(x,t) = \bar{p}(0,t) - \int_0^x \bar{G}(\xi,t) + \bar{F}(\xi,t) d\xi, \tag{16}$$

$$\bar{v}_G(x,t) = \bar{v}_G(0,t) + \int_0^x \frac{\partial \bar{v}_G(\xi,t)}{\partial \xi} d\xi. \tag{17}$$

That is, at each location $x \in [0, L]$ along the well, the terms $\bar{v}_G$ and $\bar{E}_G$ which determine the dynamics as given in (11), can be expressed as a function of either the state in the fluid column *below* x, i.e., over the interval $[0, x]$, or via the state *above* x, i.e., over the interval $[x, L]$.

An implicit expression for the inflow boundary condition at $x = 0$ can be obtained be rewriting (9)-(10) as

$$\bar{\alpha}_G(0,t) \bar{v}_G(0,t) = \frac{k_G \max(0, p_{\text{res}} - \bar{p}(0,t))}{A \bar{\rho}_G(0,t)}, \tag{18}$$

$$(1 - \bar{\alpha}_G(0,t)) \frac{\bar{v}_G(0,t) - v_\infty}{C_0} = \frac{W^{L,inj}(t)}{A \bar{\rho}_L(0,t)}, \tag{19}$$

which can be solved for $\bar{\alpha}_G(0,t)$ and $\bar{v}_G(0,t)$. Let $\bar{\alpha}_G^{\text{inflow}}(\bar{p}(0,t)) = \bar{\alpha}_G(0,t)$ be defined implicitly by the solution of (18)-(19).

III. Control design

We present an output feedback control law consisting of an observer that estimates the distributed gas concentration along the well from measurements at the topside boundary $x = L$ only, and a feedback control law that computes the topside pressure so that in closed-loop the bottom pressure at $x = 0$ convergences to the reference value p_{ref}. The control law is sampled with sampling period θ, i.e., at each time step $t_k = k\,\theta$, $k \in \mathbb{N}$, the control input is computed for the interval $[t_k, t_{k+1}]$.

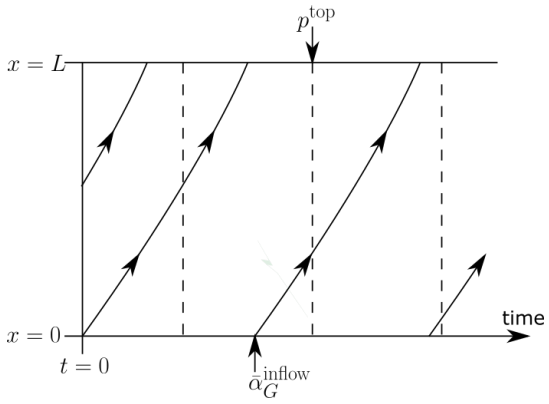

Fig. 3. Characteristic lines of system (11) representing gas propagating from the well bottom at $\boldsymbol{x = 0}$ to the top at $\boldsymbol{x = L}$. The convex curvature of the characteristic lines indicates acceleration due to expansion. The dashed lines represent the integration paths for $\bar{\boldsymbol{p}}$ and $\bar{\boldsymbol{v}}_{\boldsymbol{G}}$ as given in (14)-(17).

The control law is based on the simplified model from Section II-C. It builds on ideas from [26], [27], [36] and is also related to [25], [28], [29], [37]. In particular, it exploits the fact that the gas propagates through the well with finite speed $\bar{v}_G$ or, mathematically speaking, along the characteristic lines of the hyperbolic PDE (11) (see, e.g., [38, Chapter 2]). The characteristic lines of system (11) are sketched in Figure 3.

A. State estimation

Due to the delay corresponding to the time the gas requires to travel from the well bottom to the top, it is impossible to immediately estimate the gas concentration along the well from topside measurements. Instead, the gas outflow at the top corresponds to gas that entered at the well bottom a certain amount of time in the past.

Therefore, evaluating the proposed observer at each time step t_k consists of two steps, which are sketched in Figure 4. First, the *past* gas concentration in the well is estimated by starting with the history of topside gas concentration measurements and then solving the gas dynamics (11) *backwards* relative to how the gas propagates through the well, i.e., backwards in time and downwards in the well. Here, it is possible to reconstruct the past gas volume fraction up to the time of the characteristic line along which the latest measurement evolved (marked by the thicker line in Figure 4). Secondly, a prediction step is used to map the estimate of the past state on that characteristic line to the current state $\bar{\alpha}_G(\cdot, t_k)$.

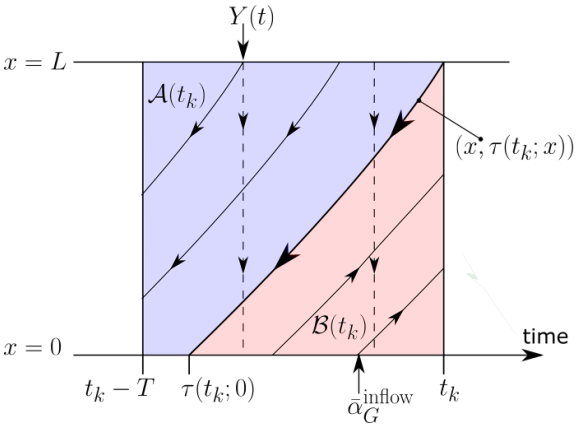

Fig. 4. Steps of evaluating the state estimation scheme at time $\boldsymbol{t_k}$: (1) Solve the dynamics (23)-(26) *against* the direction of gas propagation over the domain $\boldsymbol{\mathcal{A}(t_k)}$ (shaded in blue); (2) solve the dynamics (28)-(31) *forward* in time over the domain $\boldsymbol{\mathcal{B}(t_k)}$ (shaded in red). The thicker line represents the characteristic line $\boldsymbol{(x, \tau(t_k; x)), x \in [0, L]}$.

Define the characteristic line corresponding to the measurement at time t as

$$\tau(t; x) = t - \int_x^L \frac{1}{\bar{v}_G(\xi, \tau(t; \xi))} d\xi. \tag{20}$$

Define the measurement at time t as

$$Y(t) = \begin{pmatrix} \alpha_G(L, t) \\ p(L, t) \\ v_G(L, t) \end{pmatrix}, \tag{21}$$

and the measurement history with horizon $T > 0$ as

$$\mathbb{Y}^T(t) = \{Y(s) : s \in [t - T, t]\}. \tag{22}$$

In practice, a multi-phase flow meter can be used to measure both $\bar{\alpha}_G(L, t)$ and the topside flow rate, from which $\bar{v}_G(L, t)$ can be computed by use of (7).

1) State estimation: step 1: With the boundary values at $x = L$ known for a sufficiently long time into the past, it is possible to estimate the past state inside the well by solving the dynamics in the negative x-direction. In particular, we need to assume that $T \geq t_k - \tau(t_k; 0)$. By solving (11) for $\frac{\partial \bar{\alpha}_G}{\partial x}$ and using (14)-(15) to determine the pressure and velocity profiles, respectively, we obtain the following system:

$$\frac{\partial \bar{\alpha}_G(x, t)}{\partial x} = \frac{1}{\bar{v}_G(x, t)} \left(\bar{E}_G(x, t) - \frac{\partial \bar{\alpha}_G(x, t)}{\partial t} \right), \tag{23}$$

$$\bar{\alpha}_G(L, t) = \alpha_G(L, t), \tag{24}$$

$$\bar{p}(x, t) = p(L, t) + \int_x^L \bar{G}(\xi, t) + \bar{F}(\xi, t) d\xi, \tag{25}$$

$$\bar{v}_G(x, t) = v_G(L, t) - \int_x^L \frac{\partial \bar{v}_G(\xi, t)}{\partial \xi} d\xi. \tag{26}$$

By use of techniques similar to those in the proof of [27, Theorem 5] and [38, Theorem 3.8], one can show that the system (23)-(26) has a solution on the determinate set

$$\mathcal{A}(t_k) = \{(x, t) : x \in [0, L],\, t \in [t_k - T, \tau(t_k; x)]\}. \tag{27}$$

Importantly, the solution on $\mathcal{A}(t_k)$ contains the state on the characteristic line $(x, \tau(t_k; x))$, $x \in [0, L]$. See also [38, page

47] for a more general discussion of determinate sets, and [25, Remark 4.1] for a discussion of the minimum observation horizon T. In particular, the condition $T \geq t_k - \tau(t_k;0)$ ensures that the whole characteristic line $(x, \tau(t_k;x))$, for all $x \in [0, L]$, is contained in $\mathcal{A}(t_k)$. In other words, it ensures that the blue domain in Figure 4 reaches the bottom boundary at $x = 0$.

2) State estimation: step 2: The previous subsection provides a method for obtaining an estimate of the state on the characteristic line $(x, \tau(t_k;x))$. Starting with this estimate of the past state in the well, it is possible to estimate the current state by solving the following dynamics from $\tau(t_k;\cdot)$ up to current time t_k:

$$\frac{\partial \bar{\alpha}_G(x,t)}{\partial t} + \bar{v}_G(x,t)\frac{\partial \bar{\alpha}_G(x,t)}{\partial x} = \bar{E}_G(x,t), \tag{28}$$

$$\bar{\alpha}_G(0,t) = \bar{\alpha}_G^{\text{inflow}}\big(\bar{p}(0,t)\big), \tag{29}$$

$$\bar{p}(x,t) = \bar{p}(\tau_k^{\text{inv}}(t),t) + \int_x^{\tau_k^{\text{inv}_k}(t)} (\bar{G}+\bar{F})(\xi,t)d\xi, \tag{30}$$

$$\bar{v}_G(x,t) = \bar{v}_G(\tau_k^{\text{inv}}(t),t) - \int_x^{\tau_k^{\text{inv}}(t)} \frac{\partial \bar{v}_G(\xi,t)}{\partial x}d\xi, \tag{31}$$

where $\bar{\alpha}_G^{\text{inflow}}(\cdot)$ is defined implicitly as the solution of (18)-(19) for a given bottom hole pressure, and for given $k \in \mathbb{N}$, $\tau_k^{\text{inv}}(\cdot)$ is the inverse of $\tau(t_k;\cdot)$ in the second argument, i.e., $\tau_k^{\text{inv}}(\tau(t_k;x)) = x$. That is, for $t \in [\tau(t_k;0), t_k]$, $\tau_k^{\text{inv}}(t)$ gives the x such that $\tau(t_k;x) = t$.

Similar to above, one can show that the system (28)-(31) has a solution on the determinate set

$$\mathcal{B}(t_k) = \{(x,t) : x \in [0,L],\, t \in [\tau(t_k;x), t_k]\}. \tag{32}$$

Importantly, the solution on the set $\mathcal{B}(t_k)$ contains the estimate of the current state $\alpha(\cdot, t_k)$.

3) State estimation: algorithm: The preparations from the previous subsections provide the following algorithm for estimating the state at each sampling instance t_k, $k \in \mathbb{N}$. See also Figure 4.

Algorithm 1 State estimation algorithm

Input: measurement history $\mathbb{Y}^T(t_k)$ for $T \geq t_k - \tau(t_k;0)$
Output: estimate of state $\bar{\alpha}_G(\cdot, t_k)$

1: solve (23)-(26) in negative x-direction on $\mathcal{A}(t_k)$, to obtain estimate of past state $\bar{\alpha}_G(x, \tau(t_k,x), \bar{p}_G(x,\tau(t_k,x)$ and $\bar{v}_G(x,\tau(t_k,x)$, for all $x \in [0,L]$
2: solve (28)-(31) in positive t-direction on $\mathcal{B}(t_k)$, using the estimate from step 1. as initial condition, to obtain estimate of $\bar{\alpha}_G(\cdot, t_k)$

For all t_k satisfying $\tau(t_k;0) \geq 0$, Algorithm 1 provides an estimate of the distributed state, including gas volume fraction and pressure, in the well. If the dynamics in the well were exactly equal to the model used for observer design, (11)-(19), then these estimates would be equal to the actual state in the well. See also [25] and [36] for related state estimation results. Here, the condition $\tau(t_k;0) \geq 0$ basically requires that enough time has passed since the start of measurements, that gas has had time to travel all the way from the well bottom to the top.

Theorems showing the well-posedness and convergence of the proposed observer when applied to the simplified drift-flux model from Section II-C are summarized in Appendix I.

B. Control law

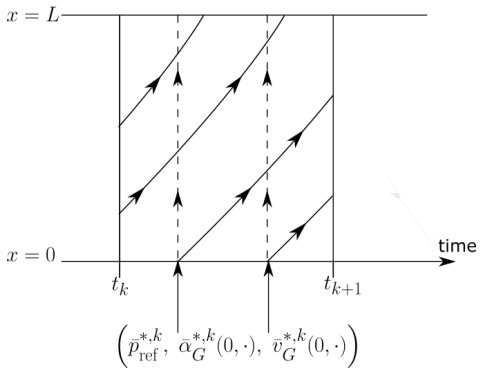

Fig. 5. Schematic of the computation of the control inputs over the interval $[\boldsymbol{t_k}, \boldsymbol{t_{k+1}}]$. Note the direction of the arrows in the dashed lines, indicating the integration path of the pressure and velocity, are in the opposite direction compared to Figure 4.

Similar to [27], [29], [36], the idea of the control design is to start with the desired bottom pressure values at $x = 0$, which shall converge to $p_{\text{ref}}(t)$ but must also be compatible with the current state, and to solve the pressure equation *against* the propagation direction of the control input, in order to compute the trajectory that satisfies these target bottom boundary values. The control input, i.e., the topside pressure, is then set equal to the topside pressure of the target trajectory.

For this purpose, let $\bar{\alpha}^{*,k}$, $\bar{p}^{*,k}$, etc., denote the target trajectory at the k-th time step, to which the system should be equal under closed-loop control. As opposed to (8), where the control input enters at the topside boundary, we introduce a new input for the target system, $p_{\text{ref}}^{*,k}$, which is the bottom hole pressure that the target trajectory shall satisfy. The target dynamics are given by

$$\frac{\partial \bar{\alpha}_G^{*,k}}{\partial t} + \bar{v}_G^{*,k}\frac{\partial \bar{\alpha}_G^{*,k}}{\partial x} = \bar{E}_G^{*,k}, \tag{33}$$

$$\bar{p}^{*,k}(x,t) = p_{\text{ref}}^{*,k}(t) - \int_0^x \bar{G}^{*,k}(\xi,t) + \bar{F}^{*,k}(\xi,t)d\xi, \tag{34}$$

$$\bar{v}_G^{*,k}(x,t) = \bar{v}_G^{*,k}(0,t) + \int_0^x \frac{\partial \bar{v}_G{*},k(\xi,t)}{\partial \xi}d\xi, \tag{35}$$

where all terms $\bar{E}_G^{*,k}$, $\bar{F}^{*,k}$, etc., are defined as in Section II-C but evaluated at the target state, and with the boundary conditions given implicitly by

$$\bar{\alpha}_G^{*,k}(0,t)\bar{v}_G^{*,k}(0,t) = \frac{k_G\ \max(0,\ p_{\text{res}} - p_{\text{ref}}^{*,k}(t))}{A\,\bar{\rho}_G^{*,k}(0,t)}, \tag{36}$$

$$\left(1 - \bar{\alpha}_G^{*,k}(0,t)\right)\frac{\bar{v}_G^{*,k}(0,t) - v_\infty}{C_0} = \frac{W^{L,inj}(t)}{A\,\bar{\rho}_L^{*,k}(0,t)}, \tag{37}$$

and initial condition

$$\bar{\alpha}_G^{*,k}(\cdot,t_k) = \bar{\alpha}_G(\cdot,t_k). \tag{38}$$

Note that the target bottom hole pressure, $p_{\text{ref}}^{*,k}$, enters in both (34) and (36).

The design of $p_{\text{ref}}^{*,k}$ must ensure continuity with the state estimate at time t_k and should converge to the actual reference, p_{ref}, in a continuous fashion. Moreover, the time derivative of $p_{\text{ref}}^{*,k}$ should remain sufficiently slow to avoid shock waves in the well or, mathematically speaking, a collision of characteristic lines. One design that satisfies these conditions is

$$p_{\text{ref}}^{*,k}(t) = \begin{cases} \bar{p}^k + \bar{p}' \cdot (t - t_k) \cdot \operatorname{sign}(e^k) & t \le t_k + \frac{|e^k|}{\bar{p}'} \\ p_{\text{ref}} & t > t_k + \frac{|e^k|}{\bar{p}'} \end{cases}, \tag{39}$$

where $\bar{p}^k = \bar{p}(0, t_k)$ and $e^k = p_{\text{ref}} - \bar{p}^k$ are the estimated bottom hole pressure and tracking error at time t_k, respectively, and $\bar{p}' > 0$ is the desired time-derivative of the bottom hole pressure. That is, $p_{\text{ref}}^{*,k}$ converges linearly with rate $\bar{p}'$ to p_{ref} and stays there once the reference is reached. If $\bar{p}'$ is chosen sufficiently small, one can again show that the system (33)-(39) is well-posed, i.e., it has a unique solution on the domain $[0, L] \times [t_k, t_{k+1}]$.

By setting

$$p^{\text{top}}(t) = \bar{p}^{*,k}(L, t) \tag{40}$$

for $t \in [t_k, t_{k+1}]$, and assuming exact model knowledge, the closed-loop trajectory of (11)-(19) is equal to the target trajectory on the domain $[0, L] \times [t_k, t_{k+1}]$. In particular, the closed loop trajectory satisfies $\bar{p}(0, t) = p_{\text{ref}}^{*,k}(t)$ for all $t \in [t_k, t_{k+1}]$. See also [27], [29], [36] for comparison.

The steps required to evaluate the control law at each time step are summarized in the following Algorithm and also in Figure 5.

Algorithm 2 Control algorithm

Input: estimate of $\bar{\alpha}_G(\cdot, t_k)$ and $\bar{p}(0, t_k)$
Output: control input $p^{\text{top}}(t)$ for $t \in [t_k, t_{k+1}]$

1: set $p_{\text{ref}}^{*,k}(t)$, $t \in [t_k, t_{k+1}]$, as per (39)
2: solve (33)-(38) over domain $[0, L] \times [t_k, t_{k+1}]$
3: set $p^{\text{top}}(t)$, $t \in [t_k, t_{k+1}]$, as per (40)

Well-posedness of the control law and convergence of the closed loop system when applied to the simplified drift-flux model from Section II-C are discussed in Appendix I.

C. Estimation of reservoir parameters

Step 1 in Algorithm 1 can also be used to estimate the production index k_G and pressure p_{res} of the reservoir, which might be uncertain in practice, using only measurements at the topside boundary. For this, note that the system (23)-(26) does not depend on the boundary condition at $x = 0$ modelling the gas influx as given by (18). That is, Step 1 in Algorithm 1 provides estimates of the bottom hole gas volume fraction and pressure, $\bar{\alpha}_G(0, t)$ and $p(0, t)$, and thus the gas influx, over the past interval $t \in [t_k - T, \tau(t_k; 0)]$, using only the history of topside measurements but not the boundary condition at the bottom of the well. In Figure 4, the time interval $t \in [t_k - T, \tau(t_k; 0)]$ corresponds to the times where the blue domain reaches the bottom boundary at $x = 0$. The uncertain values of k_G and/or p_{res} can then be estimated via standard least-square curve fitting.

For $k \in \mathbb{N}$, let $\theta_k^i \in [t_k - T, \tau(t_k; 0)]$, $i = 1, \ldots, I_k$, be sampling instances over the interval $[t_k - T, \tau(t_k; 0)]$. Let

$$\hat{w}_{G,k}^i = \bar{\alpha}_G(0, \theta_k^i)\, \bar{v}_G(0, \theta_k^i)\, \bar{\rho}_G(0, \theta_k^i)\, A, \tag{41}$$

$$\hat{p}_k^i = \bar{p}(0, \theta_k^i), \tag{42}$$

be the estimates of the gas influx and bottom hole pressure at these sampling instances as returned by step 1 in Algorithm 1. At each time step t_k, the past estimates from all previous steps up to that time can be concatenated as

$$\begin{pmatrix} \hat{W}_{G,k}^1 \\ \vdots \\ \hat{W}_{G,k}^{N_k} \end{pmatrix} = \begin{pmatrix} \hat{w}_{G,1}^1 \\ \vdots \\ \hat{w}_{G,1}^{I_1} \\ \hat{w}_{G,2}^1 \\ \vdots \\ \hat{w}_{G,2}^{I_2} \\ \vdots \\ \hat{w}_{G,k}^1 \\ \vdots \\ \hat{w}_{G,k}^{I_k} \end{pmatrix}, \quad \begin{pmatrix} \hat{P}_k^1 \\ \vdots \\ \hat{P}_k^{N_k} \end{pmatrix} = \begin{pmatrix} \hat{p}_1^1 \\ \vdots \\ \hat{p}_1^{I_1} \\ \hat{p}_2^1 \\ \vdots \\ \hat{p}_2^{I_2} \\ \vdots \\ \hat{p}_k^1 \\ \vdots \\ \hat{p}_k^{I_k} \end{pmatrix}, \tag{43}$$

where $N_k = \sum_{j=1}^k I_j$. By choosing T sufficiently large, it can be ensured that there is no gap between sampling points at consecutive steps, $\theta_k^{I_k}$ and θ_{k+1}^1. Moreover, if required the samples can be processed further to, e.g., remove duplicate samples or to ensure equal spacing.

Once the past estimates of the gas influx and bottom hole pressure have been collected, the production index and reservoir pressure can be estimated by solving the optimization problem

$$\left\{\hat{k}_G^k, \hat{p}_{\text{res}}^k\right\} = \underset{\hat{k}_G,\, \hat{p}_{\text{res}}}{\arg\min} \sum_{i=1}^{N_k} \left| \hat{W}_{G,k}^i - \hat{k}_G \max(0, \hat{p}_{\text{res}} - \hat{P}_k^i) \right|^2. \tag{44}$$

It should be noted that the curve fitting procedure does not have to be of the exactly of the form (44). For instance, weights could be put on the different samples. It is also possible to use other nonlinear functions to model the relationship between bottom hole pressure and gas influx such as polynomials of the pressure difference $\hat{p}_{\text{res}} - \hat{P}_k^i$.

D. Adding an integral term

The feedback control law in Section III-B can be seen as a static nonlinear feedback gain, similar to the proportional gain in classic linear control. In the presence of modelling errors, using such a static gain can lead to a tracking error at steady state (see also the simulations in Section IV-E). Such steady state tracking errors can be corrected if (infrequent) measurements of the bottom hole pressure are available, by adding an correction term involving the integral of the tracking error. One of the main advantages of the controller from Section III-B is that it, combined with the observer from

Section III-A, only requires topside measurements. However, some, potentially infrequent downhole pressure measurements might be available in practice, in which case it is desirable to reduce any pressure tracking errors.

Let $\tilde{t}_i$ be the sampling instances where downhole pressure measurements are available, with in general slower sampling rate $\tilde{t}_{i+1} - \tilde{t}_i \gg t_{k+1} - t_k$. Define the integral term as

$$\Pi_0 = 0, \tag{45}$$

$$\Pi_i = \Pi_{i-1} + K_I \times \left(p_{\text{ref}} - p(0, \tilde{t}_i)\right) \times \left(\tilde{t}_i - \tilde{t}_{i-1}\right), \tag{46}$$

with integral gain K_I. Then, the topside pressure as given in (40) can be modified to

$$p^{\text{top}}(t) = \bar{p}^{*,k}(L,t) + \Pi_i \tag{47}$$

for all k with $t_k \in [\tilde{t}_i, \tilde{t}_{i+1}]$. In order to avoid that the more aggressive static feedback term compensates the much slower integral term, the pressure offset must be considered in the measurement as in

$$Y(t) = \begin{pmatrix} \alpha_G(L,t) \\ p(L,t) - \Pi_i \\ v_G(L,t) \end{pmatrix}, \tag{48}$$

with i such that $t \in [\tilde{t}_i, \tilde{t}_{i+1}]$.

It should be noted that with infrequent sampling of the downhole pressure (say, in the order of once per hour), the integral term does hardly contribute to stabilization of the pressure (which would require more frequent sampling [11]), but only acts to reduce the steady state tracking error.

IV. Numerical Simulation

TABLE I
PARAMETERS

$L = 2500\,\text{m}$	$\rho_{L,0} = 975\,\text{kg/m}^3$	$p_{\text{res}} = 266\,\text{bar}$
$A = 0.012\,\text{m}^2$	$c_L = 1000\,\text{m/s}$	$k_G = 0.01\,\text{kg/(s bar)}$
$D = 0.0635\,\text{m}$	$c_G = 315\,\text{m/s}$	$W^{L,inj} = 13\,\text{kg/s}$
$f = 0.03$	$C_0 = 1.1$	$v_\infty = 0.1\,\text{m/s}$
$\theta = 10\,\text{min}$	$\bar{p}' = 10\,\text{bar/h}$	$\alpha_G(\cdot, 0) \equiv 0$

A. Simulation parameters

We demonstrate the performance of the proposed control law in numerical simulations of a well with the parameters given in Table I. The dynamics in the well are modelled using the drift-flux model introduced in Sections II-A II-B while the simplified model from Section II-C is only used for the output feedback control law. A first-order finite difference scheme with 50 discretization elements is applied to convert all PDEs (the system dynamics (2)-(4) and all PDEs in Algorithms 1 and 2) into high-order ODEs ("method of lines" [39]). The resulting ODEs are then solved in matlab by use of ode23tb.

At each sampling instance, the topside pressures are pre-computed over a $\theta = 10\,\text{minute}$ interval. The algorithm provides a continuously varying signal for the topside pressure. However, in practice, the choke on an actual rig is usually not manipulated continuously. In order to emulate this, a further zero-order hold with period 2 minutes is applied to the original topside pressure signal, so that the topside pressure becomes a piecewise-constant signal that changes every 2 minutes, and attains 5 different values over each 10 minute period. That is, due to the zero-order hold, the actual topside pressure that is applied to the system deviates slightly from the output of Algorithm 2. Pre-computing the control inputs for each 10-minute period, which involves solving the PDEs outlined in Algorithms 1 and 2, takes less than 1 second on a standard laptop, i.e., a fraction of the sampling interval.

The simulation presented below deviate from the formal analysis in Appendix I, which focuses on the simplified drift-flux model from Section II-C in closed loop with the proposed estimation and control scheme for nominal parameters, in that the simulation model is different to the model used for control design, that the control inputs are applied in a zero-order hold fashion, that the parameter identification scheme and integral action from Sections III-C and III-D are applied (which were not part of the nominal design analysed in the appendix), and that uncertainty in parameters and disturbances/noise affecting the measurements and control input are included. Thereby, the simulations serve to demonstrate that the proposed estimation and control method not only works in the ideal case, as proven in the appendix, but also shows robustness with respect to issues that need to be expected in practical applications.

B. Simulation results - nominal design

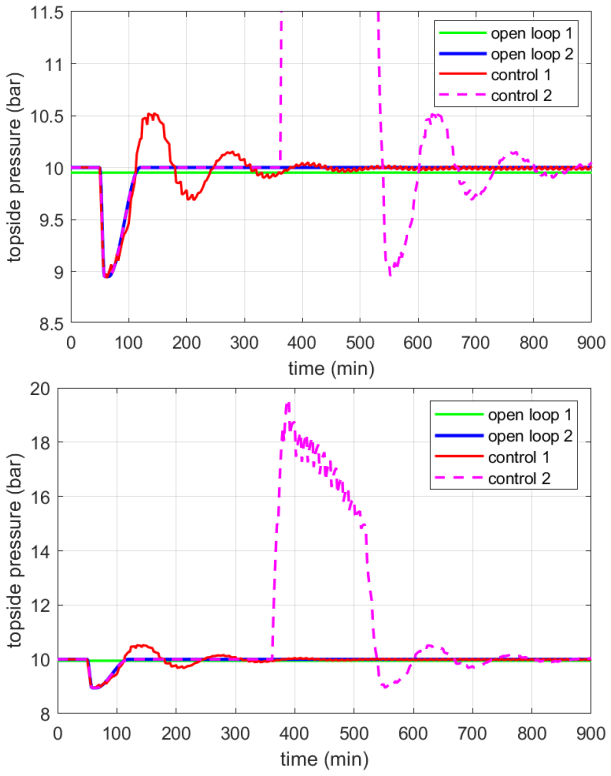

Fig. 6. Topside pressures as computed by the feedback control law presented in this paper in the two scenarios, and two open-loop alternatives. Although the topside pressures convergence to the same point, they correspond to three different equilibria, see Fig. 2. The top figure is a zoom in of the bottom figure.

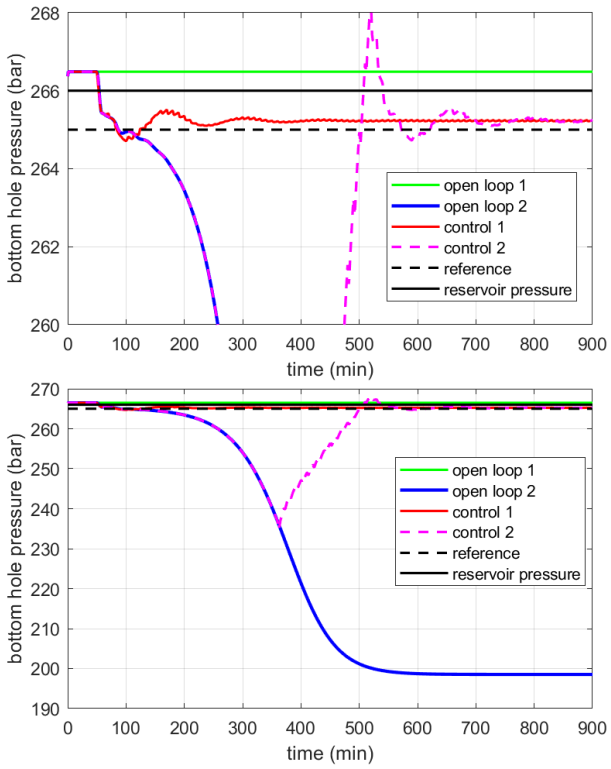

Fig. 7. Comparison of bottomhole pressure trajectories when using the proposed feedback control law in the two scenarios and the two open-loop alternatives. The top figure is a zoom in of the bottom figure.

In this section we demonstrate the controller performance in simulations where the well parameters are assumed known. The topside and bottom hole pressure trajectories are shown in Figure 6 and 7, respectively. The gas volume fraction is shown in Figure 8. At the initial condition there is no gas in the well.

In the trajectory titled "control 1", the topside pressure is initially held at 10 bar until the control law is activated at $t = 50$ minutes. While the topside pressure is at 10 bar, the bottom hole pressure sits slightly above the reservoir pressure at 266.5 bar, so that there is no inflow of gas. Once the controller is activated, it lowers the topside and, thus, the bottom hole pressure. Consequently, gas starts to enter the well. The presence of gas in the well lowers the pressure difference between topside and well bottom (because the light gas reduces the weight of the liquid/gas column), which further lowers the bottom hole pressure. The controller uses the estimate of $\bar{\alpha}_G$ to compensate this effect and stabilizes the bottom hole pressure close to the reference value at 1 bar below the reservoir pressure. Note again that the feedback controller uses no measurements of the downhole pressure, which leads to the small offset between down hole pressure reference and asymptotically achieved down hole pressure. As shown in Figure 8, once the bottom hole pressure is settled at 265 bar, the gas concentration stabilizes at around 0.3% (by area) at the well bottom and expands to approximately 6.5% at the top of the well. The controller achieves stabilization of the bottom pressure close to the reference despite the mismatch between the drift-flux model used for simulation and the simplified

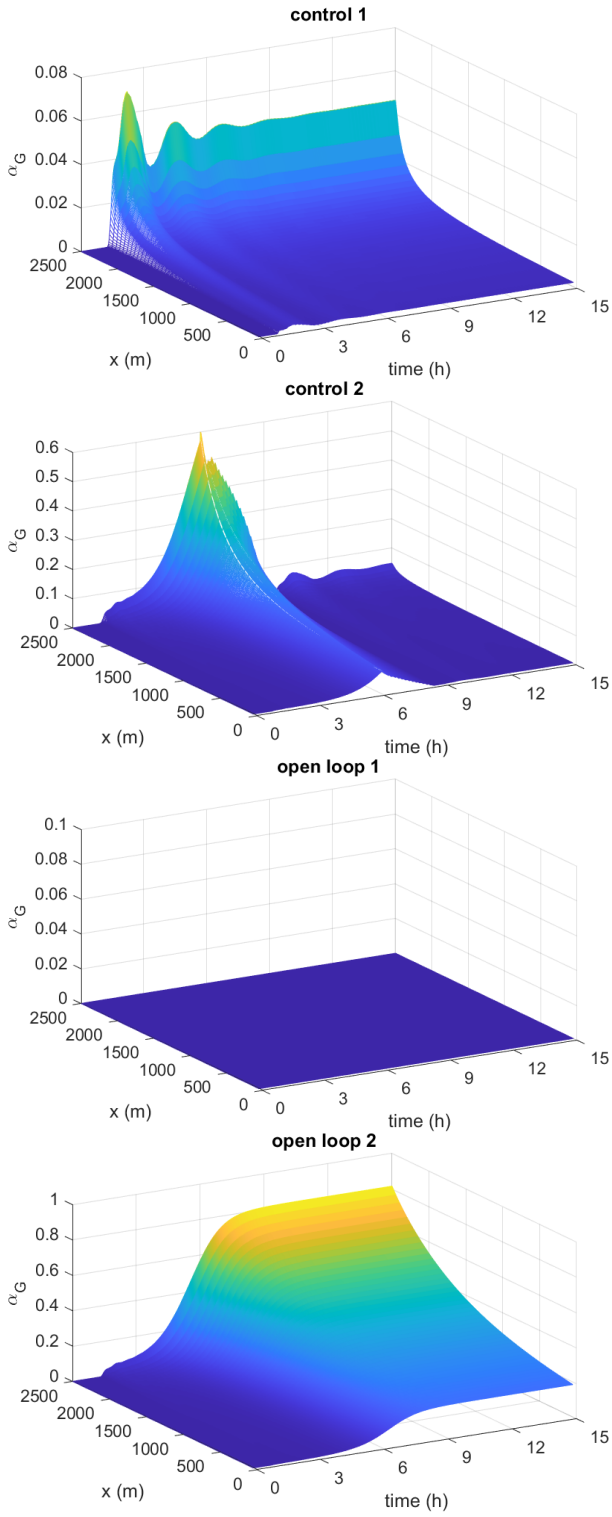

Fig. 8. Gas concentration α_G using the feedback control law presented in this paper and the two open-loop alternatives.

model used for computation of the control.

In the second closed-loop simulation ("control 2"), the feedback controller is only activated at time $t = 6$ hours. Before that, the topside pressure initially decreases as the trajectory in "control 1" in order to initiate a gas inflow, but is then eventually brought back to the equilibrium at 10 bar. This blow-out scenario is described in more detail in the following subsection under "open loop 2". Briefly speaking, the equilibrium corresponding to the reference down hole pressure is unstable, and the gas entering the well leads to a severe drop in the down hole pressure (approximately 30 bar by the time the feedback controller is activated, leading to a gas concentration of 60% at the top of the well). However, the feedback controller again manages to estimate the gas distribution in the well with sufficient accuracy, compensates its effect on the pressure in the well by increasing the topside pressure for a period of time, and brings the down hole pressure back to the reference.

In these simulations, the delay $t_k - \tau(t_k, 0)$ is just over 30 minutes at all time steps. Thus, saving the measurements over a horizon of $T = 40$ minutes is a conservative choice to ensure that the steps in Algorithm 1 are well-posed.

C. Comparison with open-loop control

For comparison, Figures 6-8 also show the trajectories corresponding to two open-loop topside pressure signals. In the first alternative ("open loop 1"), the topside pressure is held constantly at 10 bar. Since there is no gas in the well at the initial condition, the bottom hole pressure remains slightly above the reservoir pressure, i.e., in an over-balanced situation, for the entire simulation.

In the second open-loop alternative ("open loop 2"), the topside pressure signal drops like in the closed-loop simulation in order to initiate a gas inflow at the well bottom, before recovering to the average topside pressure of the closed-loop case at 10 bar. However, the equilibrium corresponding to the reference bottom hole pressure is unstable. That is, the gas inflow reduces the gravitational pressure drop in the well, which further reduces the bottom hole pressure and increases the gas inflow, until it reaches a stable equilibrium at almost 70 bar below the reference. As shown in Figure 8, the large gas influx due to the low bottom hole pressure leads to a gas concentration of approximately 18% by area at the well bottom and just over 80% at the top.

D. Estimation of reservoir parameters

In this section we demonstrate the performance of both the controller and the parameter estimation scheme from Section III-C. Here, the parameters from Table I are used to simulate the well but the reservoir parameters k_G and p_{res} are assumed to be uncertain.

Figure 9 shows the topside and bottom hole pressure trajectories for five different simulations. In three of these simulations, the initial guess $\hat{k}_G^0$ overestimates or underestimates the actual production index by 50%, respectively, and in one of them the initial guess $\hat{p}_{\text{res}}^0$ of the reservoir pressure also underestimates the actual value by 5 bar. In each

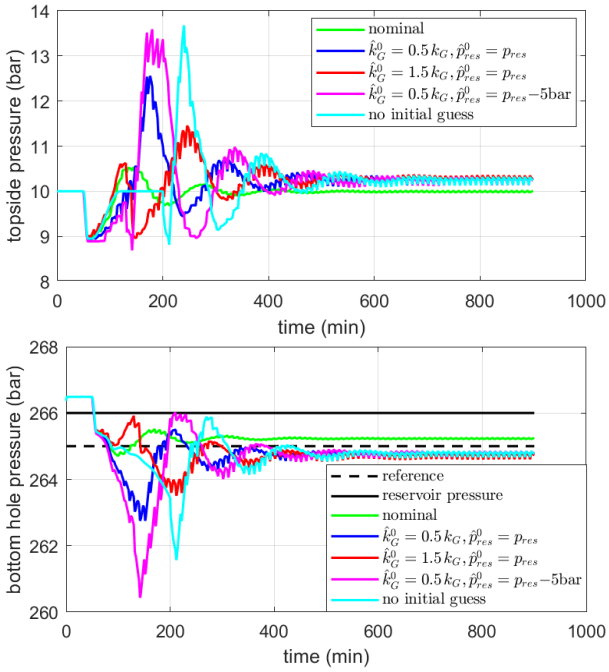

Fig. 9. Comparison of pressure trajectories for nominal and uncertain reservoir parameters.

of these simulations, the output feedback controller uses the initial values $\hat{k}_G^0$ and $\hat{p}_{\text{res}}^0$ until there is one instance at which the estimated gas influx $\hat{W}_{G,k}^i$ exceeds 1 kg/min. Once this threshold is exceeded, the reservoir parameters are estimated at each following time step as described in Section III-C based on the current set of samples, and the updated estimates $\hat{k}_G^k$ and $\hat{p}_{\text{res}}^k$ are used both Algorithm 1 for state estimation and in Algorithm 2 to compute the control inputs.

The only modification compared to Section III-C is the inclusion of a simple data processing step, in that at each t_k, the new estimation samples $\hat{w}_{G,k}^i$ and $\hat{p}_k^i$, $i = 1, \ldots, I_k$, are only added to the overall set of samples used for curve-fitting if they satisfy the following condition:

$$\min_{j \le k-1} \left| \underset{i=1\ldots I_k}{\text{mean}} (\hat{w}_{G,k}^i) - \underset{i=1\ldots I_j}{\text{mean}} (\hat{w}_{G,j}^i) \right| \ge 0.05\,\text{kg/min} \quad (49)$$

or

$$\min_{j \le k-1} \left| \underset{i=1\ldots I_k}{\text{mean}} (\hat{p}_k^i) - \underset{i=1\ldots I_j}{\text{mean}} (\hat{p}_j^i) \right| \ge 0.05\,\text{bar}. \quad (50)$$

This is to prevent that once the system settles around steady state, more and more almost identical samples of $\hat{w}_{G,k}^i$ and $\hat{p}_k^i$ keep getting added. Otherwise, excessive weight would be put on the accumulation of samples around the equilibrium, which could ultimately cause the solution of optimization problem (44) to slowly drift as more and more samples around steady state keep getting added.

In another simulation scenario, no initial guess of $\hat{k}_G^0$ and $\hat{p}_{\text{res}}^0$ is used. Instead, the topside pressure is set equal to the one used in the simulation "open loop 2" described in the previous section. As discussed above, this open-loop signal induces a gas influx and drop in the bottom hole pressure. Once the estimated gas influx $\hat{W}_{G,k}^i$ exceeds the threshold of 1 kg/min

at one sampling instance, the estimates $\hat{k}_G^k$ and $\hat{p}_{\text{res}}^k$ are again obtained as in the previous case and the feedback controller is activated. For comparison, the nominal simulation where the exact values of k_G and p_{res} are available to the controller is also shown.

As shown in Figure 9, the adaptive feedback controller manages to stabilize the bottom hole pressure close to the reference in all simulations. Uncertainty in the reservoir parameters does affect the solution during transients, before the uncertain parameters are identified. In each of the four cases with uncertainty, the estimate $\hat{k}_G^k$ settles between 7-11% below the actual value k_G, and $\hat{p}_{\text{res}}^k$ settles between 0.2-0.3 bar below p_{res}. This error leads to the slightly lower bottom hole pressures to which the four trajectories with uncertainty converge in Figure 9.

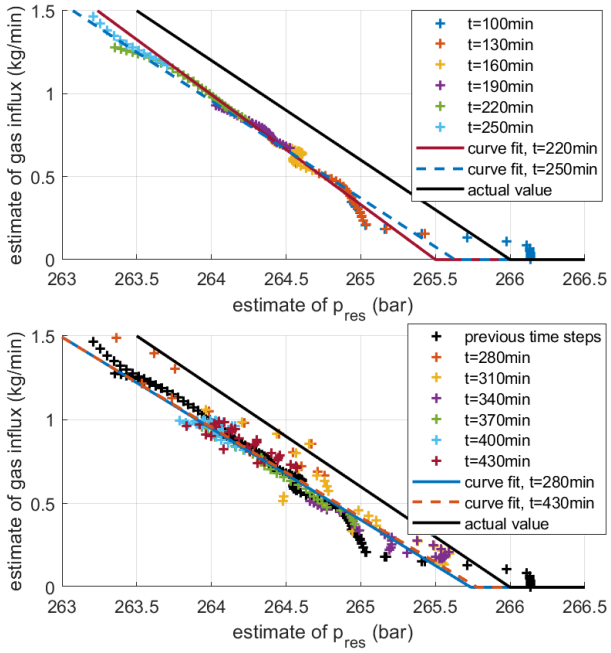

Fig. 10. Samples of gas influx estimates $\hat{\boldsymbol{w}}_{\boldsymbol{G,k}}^{\boldsymbol{i}}$ and bottom hole pressure estimates $\hat{\boldsymbol{p}}_{\boldsymbol{k}}^{\boldsymbol{i}}, \boldsymbol{i = 1, \ldots, I_k}$, at different time steps $\boldsymbol{t_k}$ (shown only for every third $\boldsymbol{t_k}$), for the simulation where no initial guesses $\hat{\boldsymbol{k}}_{\boldsymbol{G}}^{\boldsymbol{0}}$ and $\hat{\boldsymbol{p}}_{\text{res}}^{\boldsymbol{0}}$ are used. The lines show the curve fit at different times and the actual relationship as given by (9).

The parameter identification steps are investigated more closely in Figure 10, at the example of the trajectory where the system is initially operated in open-loop and no initial guesses $\hat{k}_G^0$ and $\hat{p}_{\text{res}}^0$ are used. The top figure shows samples of $\hat{w}_{G,k}^i$ and $\hat{p}_k^i$ up to time $t_k = 250$ min where the bottom hole pressure is still decreasing with time. Despite numerical errors, the samples lie close to a line (except for the very first estimated influxes up to around 0.1 kg/min), and a good curve fit is possible once the threshold of 1 kg/min is exceeded. When the pressure increases (corresponding to the samples shown in the bottom figure), the influx estimates tend to be slightly higher for the same pressure compared to when the pressure decreases. This can be attributed to numerical inaccuracies. In the bottom figure, one can also see the accumulation of samples around 264.5 bar and 0.8 kg/min for times after around $t_k = 350$ min, which is when the systems starts to settle around the equilibrium. The curve fit changes little once the maximum influx has been reached, and conditions (49)-(50) for the inclusion of new samples are not satisfied any more after $t_k = 390$ min. Compared to the actual influx as given by (9), the parameter estimation scheme tends to estimate that the same amount of gas influx occurs at a slightly lower bottom hole pressure (i.e., the estimated samples and fitted curve lie to the left of the black lines in Figure 10), which leads to the offset of approximately 0.5 bar between the adaptive simulations and the nominal simulation in Figure 9.

E. Monte Carlo Simulations

In this section we demonstrate the controller performance in Monte Carlo type simulations with parametric uncertainty and disturbances/noise affecting the measurement and actuation signals. Here, the estimation and control schemes use the nominal parameters given in Table I, whereas the actual parameters f (friction factor) and c_G (gas compressibility) used in the drift flux model vary by 5% around the nominal value. Moreover, we add a random 5% disturbance/noise signal to the topside measurement of the gas concentration, $\alpha_G(L,t)$, and another random, unmeasured disturbance to the topside pressure p^{top} of ± 0.5 bar (about 5% of 10 bar which is the nominal topside pressure). In order to vary the initial condition, the topside pressure is manually set to in between 8 bar and 10 bar, which brings the well into the under-balanced range for most parameter samples and induces a gas influx before the feedback controller is activated after 2 hours. Moreover, we show the same simulation for a shorter, 1000 m deep well. Here, the simulations are run for 100 samples in the given range, including the 18 extreme points where the uncertainty is either 0 or $\pm 5\%$ and for the initial topside pressure is either 8 bar or 10 bar, as well as 82 random samples within this range. The reference pressures are lowered compared to the previous simulations so that despite the error in the friction factor all simulations are in the under-balanced range.

The simulated trajectories are shown in Figure 11. The model errors lead to a larger offset between the achieved bottom hole pressures and reference, but the bottom hole pressures stabilize within a few bar of the reference in all simulations. The time-varying noise and disturbance terms cause some fluctuations in the pressure trajectories.

In order to compensate the steady-state tracking error, the integral term introduced in Section III-D is activated at time $t = 20$ hours with a gain of $K_I = \frac{0.1}{3600\ s}$ and sampling period of 1 hour. That is, sampling of the downhole pressure is asynchronous with the topside measurement and the integral term gets updated much less frequently than the topside pressure. Still, the integral term helps to quickly bring the bottom hole pressure close to the reference, with minor remaining fluctuations due to the noise and disturbances.

V. Conclusions

We presented a feedback control design for underbalanced drilling using only measurements and actuators located topside on the drilling rig and with uncertainty in reservoir parameters. In simulations with an industry standard drift-flux model as

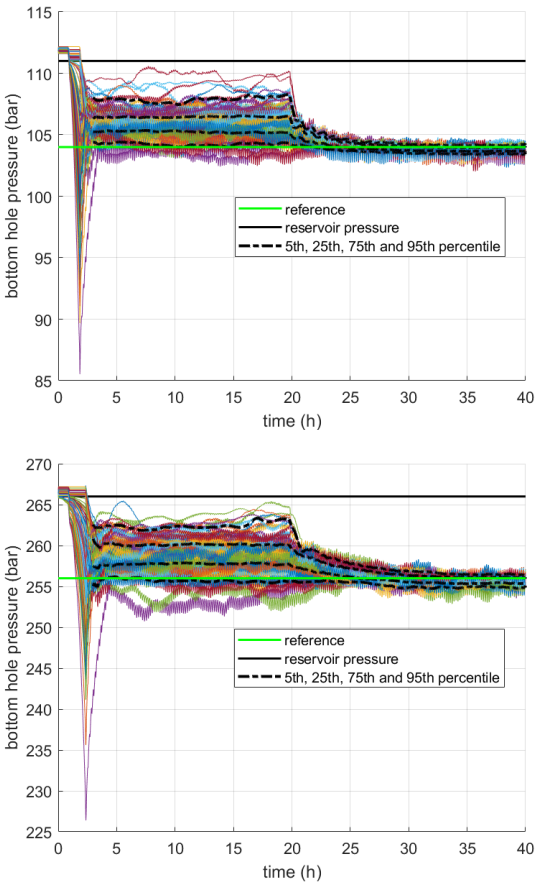

Fig. 11. Monte Carlo simulations with parametric uncertainty and disturbance/noise terms as described in the text, for the 1000 m (top) and 2500 m (bottom) deep wells. The plots show the individual bottom hole pressure trajectories (thinner lines) as well as the 5th, 25th, 75th and 95th percentiles. The integral term is activated at $\boldsymbol{t = 20}$ hours.

the plant, the proposed controller manages to stabilize the downhole pressure at an open-loop unstable setpoint slightly below the reservoir pressure (the point considered most difficult to control [4], [40]). The method also shows robustness to sampling, modelling errors and disturbances/noise affecting the topside measurements and actuation. For scenarios where infrequent measurements of the bottom hole pressure are available (in the order of once per hour), such measurements can be fed back in an integral fashion to compensate tracking errors caused by parametric uncertainty. Independently of whether the presented feedback controller or an alternative strategy is used for pressure control, the proposed estimation scheme provides estimates of the distributed gas concentration, downhole pressure, reservoir pressure, and production index using only topside measurements. Finally, the results serve as a verification that the simplified model from [35] captures the dominant dynamics of the two-phase drift flux mode that are most relevant for control design.

The simulations presented in this paper deviate to some extend from the theoretical stability analysis, in that the model used for control design is different from the plant model. Therefore, in future work the theory should be extended to close this gap. While [27] provides a conservative robustness analysis for a related system, sharper certificates for robustness with respect to model uncertainty and sampling would be highly desirable. Moreover, the stability analysis in cases with mismatch between plant model and the model used for control design would be of great interest for PDEs in general and the two versions of the drift-flux model used here in particular. Another direction for future work would be event-triggered schemes [41]–[43], which might help to further reduce the control effort by only updating the actuation when it is truly needed. For instance, using ideas from [43], the control input could be left constant as long as the predicted downhole pressure is within a band around the reference.

APPENDIX I
PROOF OF WELL-POSEDNESS AND CONVERGENCE FOR THE SIMPLIFIED DRIFT FLUX MODEL

In this section, we prove well-posedness of the observer and control law from Sections III-A and III-B, respectively, as well as stability of the closed-loop system consisting of the simplified drift-flux model (11)-(19), the observer (Algorithm 1) and the feedback control law (Algorithm 2). In order to keep the technicality of the proof manageable, some simplifying assumptions are made such as that the gas concentration is kept small and that several features from the simulations in Section IV (zero-order hold, plant-model mismatch, etc.) are neglected. Let

$$X(x,t) = \begin{pmatrix} \bar{\alpha}_G(x,t) & \bar{p}(x,t) & \bar{v}_G(x,t) \end{pmatrix}^T, \tag{51}$$

$$\tilde{X}(x,t) = \begin{pmatrix} \bar{\alpha}_G(x,t) & \bar{p}(x,t) - \bar{p}_0(x) & \bar{v}_G(x,t) - \bar{v}_{G,0}(x) \end{pmatrix}^T \tag{52}$$

$$\tilde{Y}(t) = \tilde{X}(L,t), \tag{53}$$

where $\bar{p}_0$ and $\bar{v}_{G,0}$ are the steady state pressures and velocities corresponding to zero gas concentration and $\bar{p}_0(0,t) = p_{\text{ref}}$. Note that $\frac{\partial}{\partial t}X(x,t) = \frac{\partial}{\partial t}\tilde{X}(x,t)$ for all $x \in [0,L]$.

Lemma 1: Fix $k \in \mathbb{N}$. Assume the measurements $Y(t)$ as defined in (21) is Lipschitz-continuous. There exist constants $\delta_1 > 0$ and $\delta_1' > 0$ such that if $\|\tilde{Y}(t)\| \leq \delta_1$ and $\|\frac{\partial}{\partial_t}\tilde{Y}(t)\| \leq \delta_1'$ for all $t \in [t_k - T, t_k]$ with $T > 0$ such that $\tau(t_k;0) \geq t_k - T$ (with τ as defined in (20)), then the system (23)-(26) has a unique Lipschitz-continuous solution on the domain $\mathcal{A}(t_k)$. Moreover, there exists a constant c_1' such that $\operatorname{ess\,sup}_{(x,t)\in\mathcal{A}(t_k)} \|\frac{\partial}{\partial t}X(x,t)\| \leq c_1 \operatorname{ess\,sup}_{t\in[t_k-T,t_k]} \|\frac{\partial}{\partial t}Y(t)\|$.

Proof: The proof follows the proofs of [27, Theorem 5] and [38, Theorem 3.8]. In order to define broad solutions (see [27][Theorem 3.8]), we can transform (23)-(26) into integral equations by integrating (23) along its characteristic lines. Then, by subtracting the steady state values $\bar{p}_0$ and $\bar{v}_{G,0}$, bounding the integrands by expressions that are locally Lipshitz in the state, exploiting that $\bar{p}$ in the denominator in (12) is bounded from below by $\bar{p}(x,t) \geq \bar{p}(L,t) \geq 1\,\text{bar}$ (so that $\frac{1}{\bar{p}}$ remains bounded), and using a Gronwall-type inequality, an a-priori bound on $\|\tilde{X}(x,t)\|$ for $(x,t) \in \mathcal{A}(t_k)$ can be derived. Similarly, integral equations for $\frac{\partial}{\partial t}\tilde{X}(x,t)$ can be derived, the right-hand side of which are super-linear in $\tilde{X}(t)$ and $\frac{\partial}{\partial}\tilde{X}(t)$. Using techniques as in [27, Theorem 5],

one can show that the solution of these integral equations do not blow up for all $(x,t) \in \mathcal{A}(t_k)$ if δ_1' is sufficiently small (depending on the bound on $\|\tilde{X}(x,t)\|$ derived previously). Moreover, the integral equations for $\tilde{X}$ and $\frac{\partial}{\partial t}\tilde{X}$ depend linearly on $\tilde{Y}(t)$ and $\frac{\partial}{\partial t}\tilde{Y}(t)$, respectively, which can be used to bound $\|\frac{\partial}{\partial t}X(x,t)\|$ via $\|\frac{\partial}{\partial t}Y(t)\|$. Having excluded blow-up of the solution and its time-derivative, the existence of a unique solution to the integral equations and, thus, of a broad solution to the PDE, can be proven via a fixed point argument where the local Lipschitz-continuity is used to show the contraction property. ■

Remark 2: In [27], rigorous expressions for the bounds equivalent to δ_1 and δ_1' in Lemma 1 are given for a related class of quasilinear hyperbolic systems. However, their derivations are extremely technical and are not repeated here. These bounds are based on worst-case growth estimates that are very conservative, meaning that at this stage they are unlikely to give a realistic estimate that would be of practical value. Moreover, the state X in (51) contains concentrations (< 1) and pressures ($> 10^5$ Pa). This difference in scale would lead to even more conservatism in any bounds, although this could be addressed by rescaling the state.

It is also noteworthy that in the case where the actual dynamics are equal to the ones on which Algorithm 1 is based, and the measurement corresponds to an actual, unique solution (which would be expected in practice, otherwise there is no hope of estimating the state), then all the observer does is re-solve the equations that the trajectory satisfied. In this case, the more restrictive assumptions on $\|\tilde{Y}\|$ can be relaxed, which were only introduced to ensure that the solution cannot blow up, concentrations remain below 1 etc.

The same techniques as in Lemma 1 can be used to show well-posedness of the second step in the observer evaluation.

Lemma 3: Assume $X(x,\tau(t_k;x))$ is Lipshitz-continuous in $x \in [0,L]$. There exist constants $\delta_2 > 0$ and $\delta_2' > 0$ such that if $\sup_{x\in[0,L]} \|\tilde{X}(x,\tau(t_k;x))\| \leq \delta_2$ and $\operatorname{ess\,sup}_{x\in[0,L]} \|\frac{\partial}{\partial_t}\tilde{X}(x,\tau(t_k;x))\| \leq \delta_2'$, then the system (28)-(31) has a unique solution on the domain $\mathcal{B}(t_k)$.

Lemmas 1 and 3 form the basis for showing well-posedness and convergence of the observer defined in Algorithm 1.

Theorem 4: Assume the measurements $Y(t)$ is Lipschitz-continuous for all t. There exist $K \in \mathbb{N}$ and constants $\delta_3 > 0$ and $\delta_3' > 0$ such that if $\|\tilde{Y}(t)\| \leq \delta_3$ and $\|\frac{\partial}{\partial_t}\tilde{Y}(t)\| \leq \delta_3'$ for all $t \in [0,\infty)$, then the state estimate obtained by Algorithm 1 is equal to the actual state at all times t_k with $k \geq K$.

Proof: One can choose K large enough such that $\tau(t_K;0) > 0$. Since both the actual and the estimated trajectory satisfy (23)-(26) and are equal to Y at $x = L$, uniqueness of the solution on $\mathcal{A}(t_k)$ for $k \geq K$ as guaranteed by Lemma 1, implies that the estimated state is equal to the actual on all of $\mathcal{A}(t_k)$, including on the characteristic line $(x,\tau(t_k;x))$, $x \in [0,L]$. Similarly, since the observer equations (28)-(31) are just a copy of the set of equations that the actual dynamics satisfy, Lemma 3 implies that the estimated and actual state exist and are equal on $\mathcal{B}(t_k)$ if $\|\tilde{X}(x,t)\|$ and $\|\frac{\partial}{\partial t}\|\tilde{X}(x,t)\|$ are sufficiently small on the line $(x,\tau(t_k;x))$, $x \in [0,L]$. By the last statement in Lemma 1, the latter can be ensured by choosing δ_3 and δ_3' sufficiently small. Since $\mathcal{B}(t_k)$ includes the line (x,t_k), $x \in [0,L]$, this implies that the estimate of $X(\cdot,t_k)$ is equal to the actual value. ■

We next formulate a lemma regarding well-posedness of each feedback control step as given by Algorithm 2.

Lemma 5: Fix $k \in \mathbb{N}$ and assume the state at time t_k is fully known, i.e., (38) is satisfied. There exist $\delta_4 > 0$ and $\delta_4' > 0$ and $\bar{\delta} > 0$ such that if $\|\tilde{X}(\cdot,t_k)\|_\infty \leq \delta_4$, $\|\frac{\partial}{\partial t}\tilde{X}(\cdot,t_k)\|_\infty \leq \delta_4'$ and $\bar{p}' \leq \bar{\delta}$, then (33)-(38) has a unique solution on $(x,t) \in [0,L] \times [t_k,t_{k+1}]$. Moreover, the actual system (11)-(19) in closed loop with p^{top} as constructed by Algorithm 2 satisfies $\bar{p}(0,t) = p_{\text{ref}}^{*,k}(t)$ for all $t \in [t_k,t_{k+1}]$.

Proof: Existence and uniqueness of the solution on $(x,t) \in [0,L] \times [t_k,t_{k+1}]$ can be proven using the same techniques as in Lemma 1, where we again use that (33)-(38) is just a reformulated version of the actual dynamics. In particular, uniqueness of the solution includes that $\bar{p}(x,t) = \bar{p}^{*,k}(x,t)$ on $(x,t) \in [0,L] \times [t_k,t_{k+1}]$. That is, $\bar{p}(0,t) = p_{\text{ref}}^{*,k}(t)$ for all $t \in [t_k,t_{k+1}]$ if and only if $\bar{p}(L,t) = p^{\text{top}}(t) = \bar{p}^{*,k}(L,t)$ for all $t \in [t_k,t_{k+1}]$. ■

We are now in position to prove the main theorem on well-posedness and convergence of the closed loop system.

Theorem 6: Assume the feedback controller is activated at some time T with $\tau(T;0) \geq 0$. There exist $\delta_5 > 0$, $\delta_5' > 0$, $\tilde{\delta}_5 > 0$, $\tilde{\delta}_5' > 0$, $\bar{\delta} > 0$ and $T' > T$ such that if the initial conditions and $p^{\text{top}}(t)$ for $t \leq T$ are Lipschitz continuous, compatible and such that the solution exists up to time T with $\|\tilde{Y}(t)\| \leq \tilde{\delta}_5$ and $\|\frac{\partial}{\partial_t}\tilde{Y}(t)\| \leq \tilde{\delta}_t'$ for all $t \leq T$, and such that $\|\tilde{X}(\cdot,T)\|_\infty \leq \delta_5$ and $\|\frac{\delta}{\delta t}\tilde{X}(\cdot,T)\|_\infty \leq \delta_5'$, then the closed-loop system consisting of the simplified drift flux model (11)-(19), the observer in Algorithm 1 and the feedback control law in Algorithm 2 with $\bar{p}' \leq \bar{\delta}$ has a unique solution on $[0,L] \times [0,\infty)$ that satisfies $\bar{p}(0,t) = p_{\text{ref}}$ for all $t \geq T'$.

Proof: Since $\tau(T;0) \geq 0$ by assumption, Theorem 4 states that the observer has converged by the time the feedback controller is activated. Here, it is assumed that the initial conditions and $p_{\text{top}}(t)$ for $t \leq T$ are benign such that the system is actually observable and controllable by the time the controller is activated. For all k with $t_k \geq T$, by Lemma 5 the solution satisfies $\bar{p}(0,t) = p_{\text{ref}}^{*,k}(t)$ for $t \in [t_k,t_{k+1}]$. By recursively using the design in Equation (39), this means that $\bar{p}(0,t) = p_{\text{ref}}^{*,k}(t) = p_{\text{ref}}$ for all $t \geq T' = \frac{|\bar{p}(0,T) - p_{\text{ref}}|}{\bar{p}'}$. With regards to well-posedness, the design in (39) and the assumption that $\|\tilde{X}(\cdot,T)\|_\infty \leq \delta_5$, ensures that $\bar{p}(0,t) = p_{\text{ref}}^{*,k}$ remains below a bound that can be made arbitrarily small by making δ_5 small. The norm of the time derivative at $x = 0$, $\|\frac{\partial}{\partial t}\tilde{X}(0,t)\|$ for $t \geq T$ can be made arbitrarily small via $\bar{p}'$. Then, similar as in Lemma 1, by solving the dynamics in the positive x-direction with the "initial" condition at $x = 0$, one can show that this implies that $\|\tilde{X}(x,t)\|$ and $\|\frac{\partial}{\partial t}\tilde{X}(x,t)\|$ remain sufficiently small for all $x \in [0,L]$, $t \geq T$. That is, the solution cannot blow up in finite time, and the assumptions of Theorem 4 (smallness of $\|\tilde{Y}(t)\|$ and $\|\frac{\partial}{\partial_t}\tilde{Y}(t)\|$) and Lemma 5 (smallness of $\|\tilde{X}(\cdot,t_k)\|_\infty$ and $\|\frac{\partial}{\partial t}\tilde{X}(\cdot,t_k)\|_\infty$) are recursively satisfied. Moreover, the design (39) is such that $p_{\text{ref}}^{*,k}(t_k) = \bar{p}(0,t_k)$ which, due to (14)/(16) and (34), implies that $p_{\text{top}}(t)$ stays continuous at $t = t_k$ for all k so that the whole solution remains Lipschitz-continuous. ■

Remark 7: In [27], rigorous, although quite conservative certificates for robustness with respect to uncertainty in parameters and measurement and actuation inaccuracies are given for a related class of quasilinear hyperbolic systems. Deriving similar conditions for the system considered here would go beyond the scope of this paper. However, the numerical simulations in Section IV-E suggest that there is some inherent robustness with respect to such uncertainties, as well as with respect to mismatch between the full drift-flux model and the siomplified model used for control design. The assumptions in Theorem 6, in particular smallness of the state $\tilde{X}$, are conservative and are made to simplify the proof of existence of the solution, i.e., that the solution cannot escape in finite time, that concentrations remain below 1, etc. Hypothetically, if existence and uniqueness of the solution that is equal to the open-loop trajectory up to time T and from then onwards satisfies $\bar{p}(0,t) = p_{\text{ref}}^{*,k}(t)$, was guaranteed a priori, then all Algorithm 2 does is compute the corresponding topside pressures. In that sense, smallness of $\|\tilde{X}\|$ is a conservative sufficient condition rather than a necessary one.

The sampling period θ does not appear in Theorem 6 because in the appendix, exact model knowledge and predictability are assumed. In presence of model uncertainty, the sensitivity of closed-loop stability with respect to θ is also investigated in [27]. In particular, long θ can reduce the robustness with respect to model uncertainty due to prediction errors, while very short θ can also be detrimental because new measurement errors are introduced at every sampling event. The latter can be managed by introducing a minimum dwell time (see also the classical reference [44]).

REFERENCES

[1] J.-M. Godhavn, "Control Requirements for Automatic Managed Pressure Drilling System," *SPE Drilling & Completion*, vol. 25, no. 3, pp. 336–345, apr 2010.

[2] J. M. Godhavn, A. Pavlov, G. O. Kaasa, and N. L. Rolland, "Drilling seeking automatic control solutions," in *IFAC Proceedings Volumes (IFAC-PapersOnline)*, B. Sergio, Ed., vol. 18, no. PART 1, Milano, Italy, aug 2011, pp. 10 842–10 850.

[3] D. B. Bennion, F. B. Thomas, R. F. Bietz, and D. W. Bennion, "Underbalanced Drilling, Praises and Perils," in *Permian Basin Oil and Gas Recovery Conference*, no. December. Society of Petroleum Engineers, apr 1996.

[4] R. A. Graham and M. S. Culen, "Methodology For Manipulation Of Wellhead Pressure Control For The Purpose Of Recovering Gas To Process In Underbalanced Drilling Applications," in *Proceedings of SPE/IADC Underbalanced Technology Conference and Exhibition*. Houston, Texas: Society of Petroleum Engineers, oct 2004.

[5] U. J. F. Aarsnes, F. Di Meglio, O. M. Aamo, and G.-O. Kaasa, "Fit-for-Purpose Modeling for Automation of Underbalanced Drilling Operations," in *SPE/IADC Managed Pressure Drilling & Underbalanced Operations Conference & Exhibition*. Madrid, Spain: Society of Petroleum Engineers, apr 2014, pp. SPE–168 955–MS.

[6] C. Mykytiw, I. Davidson, and P. Frink, "Design and Operational Considerations to Maintain Underbalanced Conditions with Concentric Casing Injection," in *IADC/SPE Underbalanced Technology Conference and Exhibition*. Society of Petroleum Engineers, apr 2003.

[7] C. Mykytiw, P. Suryanarayana, and P. Brand, "Practical Use of a Multiphase Flow Simulator for Underbalanced Drilling Applications Design - The Tricks of the Trade," in *SPE/IADC Underbalanced Technology Conference and Exhibition*. Society of Petroleum Engineers, apr 2004.

[8] U. J. F. Aarsnes, "Modeling of Two-Phase Flow for Estimation and Control of Drilling Operations," Ph.D. dissertation, Norwegian University of Science and Technology, 2016.

[9] U. J. F. Aarsnes, F. Di Meglio, R. Graham, and O. M. Aamo, "A methodology for classifying operating regimes in underbalanced-drilling operations," *SPE Journal*, vol. 21, no. 02, pp. 423–433, 2016.

[10] T. Pedersen and J.-M. Godhavn, "Model Predictive Control of Flow and Pressure in Underbalanced Drilling," in *10th IFAC International Symposium on Dynamics and Control of Process Systems (2013)*, 2013, pp. 307–312.

[11] T. Pedersen, U. J. F. Aarsnes, and J.-m. Godhavn, "Flow and pressure control of underbalanced drilling operations using NMPC," *Journal of Process Control*, vol. 68, pp. 73–85, 2018.

[12] T. Pedersen and J.-m. Godhavn, "Linear Multivariable Control of Underbalanced-Drilling Operations," *SPE Drilling & Completion*, vol. 32, no. 04, pp. 1–11, 2017.

[13] T. Pedersen, J.-M. Godhavn, and J. Schubert, "Supervisory control for underbalanced drilling operations," *IFAC-PapersOnLine*, vol. 48, no. 6, pp. 120–127, 2015.

[14] M. Krstic and A. Smyshlyaev, "Backstepping boundary control for first-order hyperbolic PDEs and application to systems with actuator and sensor delays," *Systems & Control Letters*, vol. 57, no. 9, pp. 750–758, 2008.

[15] R. Vazquez, M. Krstic, and J.-M. Coron, "Backstepping boundary stabilization and state estimation of a 2× 2 linear hyperbolic system," in *2011 50th IEEE Conference on Decision and Control and European Control Conference (CDC-ECC)*, 2011, pp. 4937–4942.

[16] O. M. Aamo, "Disturbance rejection in 2×2 linear hyperbolic systems," *IEEE Transactions on Automatic Control*, vol. 58, no. 5, pp. 1095–1106, 2013.

[17] P.-O. Lamare and N. Bekiaris-Liberis, "Control of 2× 2 linear hyperbolic systems: Backstepping-based trajectory generation and pi-based tracking," *Systems & Control Letters*, 2015.

[18] P.-O. Lamare and F. Di Meglio, "Adding an integrator to backstepping: Output disturbances rejection for linear hyperbolic systems," in *2016 American Control Conference (ACC)*. IEEE, 2016, pp. 3422–3428.

[19] S. Pohjolainen, "Robust multivariable pi-controller for infinite dimensional systems," *IEEE Transactions on Automatic Control*, 1982.

[20] J.-M. Coron and A. Hayat, "Pi controllers for 1-d nonlinear transport equation," *IEEE Transactions on Automatic Control*, 2019.

[21] V. Dos Santos, G. Bastin, J.-M. Coron, and B. d'Andréa Novel, "Boundary control with integral action for hyperbolic systems of conservation laws: Stability and experiments," *Automatica*, 2008.

[22] M. Barreau, F. Gouaisbaut, and A. Seuret, "Practical stability analysis of a drilling pipe under friction with a pi-controller," *IEEE Transactions on Control Systems Technology*, 2019.

[23] H. Lhachemi, C. Prieur, and E. Trélat, "Pi regulation of a reaction–diffusion equation with delayed boundary control," *IEEE Transactions on Automatic Control*, 2020.

[24] H. Lhachemi, A. Malik, and R. Shorten, "Integral action for setpoint regulation control of a reaction–diffusion equation in the presence of a state delay," *Automatica*, 2021.

[25] T. Li, "Exact boundary observability for quasilinear hyperbolic systems," *ESAIM: Control, Optimisation and Calculus of Variations*, vol. 14, no. 4, pp. 759–766, 2008.

[26] T. Strecker, O. M. Aamo, and M. Cantoni, "Direct predictive boundary control of a first-order quasilinear hyperbolic PDE," in *2019 IEEE 58th Annual Conference on Decision and Control (CDC)*. IEEE, 2019.

[27] ——, "Boundary feedback control of 2x2 quasilinear hyperbolic systems: Predictive synthesis and robustness analysis," *IEEE Transactions on Automatic Control*, 2021.

[28] T.-T. Li and B.-P. Rao, "Exact boundary controllability for quasilinear hyperbolic systems," *SIAM Journal on Control and Optimization*, vol. 41, no. 6, pp. 1748–1755, 2003.

[29] M. Gugat, M. Herty, and V. Schleper, "Flow control in gas networks: exact controllability to a given demand," *Mathematical Methods in the Applied Sciences*, vol. 34, no. 7, pp. 745–757, 2011.

[30] U. J. F. Aarsnes, F. Di Meglio, S. Evje, and O. M. Aamo, "Control-oriented drift-flux modeling of single and two-phase flow for drilling," in *ASME 2014 Dynamic Systems and Control Conference*, vol. 3. San Antonio, Texas, USA: ASME, oct 2014, p. V003T37A003.

[31] S. Evje and K. K. Fjelde, "Hybrid Flux-Splitting Schemes for a Two-Phase Flow Model," *Journal of Computational Physics*, vol. 175, no. 2, pp. 674–701, jan 2002.

[32] U. J. F. Aarsnes, T. Flåtten, and O. M. Aamo, "Review of two-phase flow models for control and estimation," *Annual Reviews in Control*, vol. 42, pp. 50–62, jul 2016.

[33] J. E. Udegbunam, K. K. Fjelde, S. Evje, and G. Nygaard, "On the Advection-Upstream-Splitting-Method Hybrid Scheme: A Simple Transient-Flow Model for Managed-Pressure-Drilling and

Underbalanced-Drilling Applications," *SPE Drilling & Completion*, vol. 30, no. 02, pp. 098–109, jun 2015.

[34] S. Gavrilyuk and J. Fabre, "Lagrangian coordinates for a drift-flux model of a gas-liquid mixture," *International journal of multiphase flow*, vol. 22, no. 3, pp. 453–460, 1996.

[35] U. J. F. Aarsnes, A. Ambrus, F. Di Meglio, A. K. Vajargah, O. M. Aamo, and E. van Oort, "A simplified two-phase flow model using a quasi-equilibrium momentum balance," *International Journal of Multiphase Flow*, vol. 83, pp. 77–85, 2016.

[36] T. Strecker and O. M. Aamo, "Output feedback boundary control of 2×2 semilinear hyperbolic systems," *Automatica*, vol. 83, pp. 290–302, 2017.

[37] T. Li, K. Wang, and Q. Gu, *Exact Boundary Controllability of Nodal Profile for Quasilinear Hyperbolic Systems*. Springer, 2016.

[38] A. Bressan, *Hyperbolic systems of conservation laws: the one-dimensional Cauchy problem*. Oxford University Press, 2000, vol. 20.

[39] J. G. Verwer and J. M. Sanz-Serna, "Convergence of method of lines approximations to partial differential equations," *Computing*, vol. 33, no. 3, pp. 297–313, 1984.

[40] B. Guo and A. Ghalambor, "An Innovation in Designing Underbalanced Drilling Flow Rates: A Gas-Liquid Rate Window (GLRW) Approach," in *Proceedings of IADC/SPE Asia Pacific Drilling Technology*. Society of Petroleum Engineers, sep 2002.

[41] W. P. Heemels, K. H. Johansson, and P. Tabuada, "An introduction to event-triggered and self-triggered control," in *51st conference on decision and control*. IEEE, 2012.

[42] N. Espitia, "Observer-based event-triggered boundary control of a linear $2\times$ 2 hyperbolic systems," *Systems & Control Letters*, vol. 138, p. 104668, 2020.

[43] T. Strecker, M. Cantoni, and O. M. Aamo, "Event-triggered boundary control of 2×2 semilinear hyperbolic systems," *Preprint available at: https://arxiv.org/abs/2203.09061*, 2022.

[44] J. P. Hespanha and A. S. Morse, "Stability of switched systems with average dwell-time," in *38th IEEE conference on decision and control*. IEEE, 1999.